Rheol Acta (2008) 47:283–300
DOI 10.1007/s00397-008-0260-9

REVIEW

# Perspectives on shear banding in complex fluids

**Peter D. Olmsted**

Received: 12 December 2007 / Accepted: 15 January 2008 / Published online: 7 March 2008


**Abstract** In this review, I present an idiosyncratic view of the current state of shear banding in complex fluids. Particular attention is paid to some of the outstanding issues and questions facing the field, including the applicability of models that have "traditionally" been used to model experiments; future directions and challenges for experimentalists; and some of the issues surrounding vorticity banding, which has been discussed theoretically and whose experiments are fewer in number yet, in many ways, more varied in character.

**Keywords** Constitutive instabilities · Shear-induced structure formation · Shear banding · Shear thinning · Nonlinear viscoelasticity · Spatiotemporal structure formation

## Introduction

Shear banding has been studied for a few decades, and it occurs in complex fluids with structure that relaxes on slow time scales (Olmsted and Lu 1999b; Fielding 2007). When an imposed shear rate exceeds a characteristic structural relaxation time, the fluid can attain a nonequilibrium state whose structure is qualitatively different from that of the quiescent state. If the resulting new structure has a different apparent viscosity, the rheological feedback can lead to an inhomogeneous state in which "shear bands" of fluids with different apparent viscosities coexist, separated along the flow gradient direction ("*gradient banding*") and having the same shear stress. Similar situations are possible for imposed shear stresses, in which case the system can separate, in principle, into bands of different stress along the vorticity direction *vorticity banding*. Gradient banding is by far the best studied example, and it occurs in many different complex fluids (Fielding 2007); within this class of shear banding, wormlike micellar surfactant solutions have been the best studied (Rehage and Hoffmann 1991; Berret 2005; Cates and Fielding 2006).

A simple interpretation of gradient shear banding is a coexistence of two macroscopic regions, or shear bands, of materials flowing at different shear rates for a given imposed stress, and thus possessing different apparent viscosities and different states of microstructural organization. These bands are thought to represent stable branches of the fluid's *constitutive curve*. The constitutive curve is defined as the steady state relation between total shear stress and shear rate that would be observed *if the system were homogeneous*. In most gradient banding systems the induced phase has a lower viscosity, so that the constitutive curve is posited to resemble a van der Waals loop, with a region of total stress for which two locally stable shear rates and one unstable shear rate exist. For imposed shear rates in the unstable region, the homogeneous state is unstable and thus breaks up into a stable inhomogeneous state in which the two bands are stable and separated by an interface. A similar construction is possible when flow induces a constitutive branch that over- or underhangs the quiescent flow branch (Olmsted 1999). Figure 2 summarize some of the possible situations.

This simple interpretation arises from the earliest experiments, beginning in the 1990s, in which

P. D. Olmsted (✉)
School of Physics & Astronomy, University of Leeds,
Leeds, LS2 9JT, UK
e-mail: p.d.olmsted@leeds.ac.uk

inhomogeneous states were first interpreted from the measured rheology (Rehage and Hoffmann 1991; Spenley et al. 1993; Schmitt et al. 1994), and then verified from experiments, such as NMR imaging to measure the velocity profile (Callaghan et al. 1996; Britton and Callaghan 1999) or birefringence to detect macroscopic regions of different degrees of orientational order (Decruppe et al. 1995). More recently, techniques with much better spatial and temporal resolution have been developed, such as more precise NMR imaging (Raynaud et al. 2002; Holmes et al. 2003), particle imaging velocimetry (Hu and Lips 2005; Wang et al. 2006), ultrasound velocimetry (Manneville et al. 2004a; Becu et al. 2004), heterodyne dynamic light scattering (Salmon et al. 2003b; Manneville et al. 2004a), and optical microscopy and scattering (Wheeler et al. 1998; Lerouge et al. 2006; Fischer et al. 2002; Ganapathy and Sood 2006a). These newest measurements show that in many, if not most, shear banding situations, the high-shear-rate band is very dynamic and possibly unstable. Hence, the simple picture may in many cases be a time-average of the true situation. This has since spurred theoretical studies to address nonsteady, chaotic, and unstable flows (Chakrabarti et al. 2004; Forest et al. 2004; Aradian and Cates 2005; Fielding and Olmsted 2004, 2006; Fielding 2005; Wilson and Fielding 2006). One recent result is that the Johnson–Segalman (JS) model, which continues to be used as a simple and somewhat tractable model to describe shear banding, has an inherent instability with respect to the "canonical" one-dimensional shear banding state (Fielding 2005; Wilson and Fielding 2006). This may or may not help explain some of the experiments that show how some wormlike micelle solutions have an inherent dynamical high-shear-rate state (Holmes et al. 2003; Becu et al. 2004; Lerouge et al. 2006; Decruppe et al. 2006; Bandyopadhyay et al. 2000; Lopez-Gonzalez et al. 2004).

Hence, the advent of techniques of continually increasing resolution is forcing the field to rethink some of the basic ideas of shear banding that have been developed over the past decade, leading to many questions: Is a one-dimensional steady-state banding picture overly naive? Is there an adequate constitutive model to describe wormlike micelles? Furthermore, very little is still known theoretically about shear-thickening systems such as dilute surfactant solutions of wormlike micelles (Hu et al. 1998a; Herle et al. 2005) and lamellar surfactant solutions that form onions (Diat et al. 1993; Bonn et al. 1998; Wunenburger et al. 2001; Salmon et al. 2002; Panizza et al. 1998; Roux et al. 1993; Bergenholtz and Wagner 1996; Leon et al. 2000).

In this review, I will present, primarily, some of the outstanding issues in understanding shear banding. I will avoid overlap with other recent reviews on complex dynamics and instabilities in shear banding (Fielding 2007) or on wormlike micelles (Cates and Fielding 2006), but refer the interested reader to these excellent surveys. Hence, I will give a brief summary of some of the experiments, followed by a detailed discussion of "stress selection" and its implications, as well as some details about what is and is not known about vorticity banding, a poorly understood and little-studied corner of the field. I also collect together a few of the theoretical models that describe shear banding.

## Overview of experiments and phenomena

The reader is urged to consult Fielding (2007) for an excellent recent review of shear banding experiments. As mentioned above, many complex fluid solutions exhibit shear banding. Here, I give a rather cursory tour through some of the most studied systems; unfortunately, no attempt has been made to be comprehensive, for which I apologize!

### Wormlike micelles

Shear banding is seen in many surfactant and amphiphilic solutions, probably because these systems form delicate and complex structures that are thus easily perturbed by flow. Perhaps the best-studied example is solutions of wormlike micelles (Rehage and Hoffmann 1991; Cates and Fielding 2006; Schmitt et al. 1994; Berret et al. 1994; Cates and Candau 1990). The variety of behavior exhibited by these systems is staggering. In the best-studied examples, flow induces a low-viscosity phase in which the micelles are aligned close to the flow direction (Schmitt et al. 1994; Berret et al. 1994, 1997; Cappelaere et al. 1997). This can either be in dilute solutions, where the shear banding transition is thought to be due to the viscoelastic effects of entangled polymer solutions (Cates 1990; Doi and Edwards 1989), or in more concentrated systems near the isotropic-nematic transition (Roux et al. 1995). The basic physics behind shear banding in dilute solutions is thought to be that of entangled polymer solutions: upon shearing faster than the characteristic relaxation time, which is a combination of reptation and micellar breakage, a stress maximum leads to a runaway instability to a high-shear-rate phase which, while poorly understood or characterized, is typically highly birefringent, and this comprises a highly oriented structure. In more concentrated solutions, liquid crystalline effects

undoubtedly contribute to the instability. Although there has been some discussion of whether "mechanical" or "thermodynamic" effects dominate (Schmitt et al. 1995; Porte et al. 1997; Fielding and Olmsted 2003a), in practice there is little difference between the two: a first-order phase transition typically has associated mechanical instabilities (such as a negative bulk modulus at the ordinary liquid-vapor phase transition and a negative differential shear viscosity at the flow-induced isotropic-to-nematic phase transition).

However, it is important to identify the important microscopic mechanisms of flow-structure coupling: possibilities include entanglement effects, micellar breakage or enhanced length, liquid–crystalline effects, changes in charge and association, or other changes in micellar topology. Unfortunately, there remains little known about these effects, and observation of these issues is an outstanding experimental challenge. Two interesting recent experiments that may help in this respect are an NMR measurement that inferred a change in surfactant tail order in shear, perhaps consistent with an induced tension in the micelles Holmes et al. (2004b), and a study that compared the effect of changing the micellar breakage time at fixed overall relaxation time; this changed the nature of the observed hysteresis at the low shear rate edge of the stress plateau and also influenced the stress fluctuations on the stress plateau (Pimenta and Pashkovski 2006).

More dilute systems exhibit a shear thickening transition, which also remains poorly understood (Hu et al. 1998a, b; van Egmond 1998; Berret et al. 1998), despite considerable work. Very dilute solutions, with a quiescent viscosity close to that of the solvent, can be induced to thicken dramatically and, at times, induce shear banding. Despite scattering that shows large shear-induced structures (Hu et al. 1998a, b; Berret et al. 1998; Gamez-Corrales et al. 1999; Boltenhagen et al. 1997), as well as cryo-microscopy (Keller et al. 1998), the nature of the thickened state remains elusive. Suggestions have included runaway growth of linear micelles (Cates and Turner 1990; Bruinsma et al. 1992), formation and breakage of ultra-long "olympic ring" structures stabilized by large end cap energies (Cates and Candau 2001), and the influence of flow on electrostatically driven bundling (Barentin and Liu 2001). This remains an unresolved issue.

Most micellar shear banding transitions have been gradient banding, as in Fig. 1a, b. However, because the

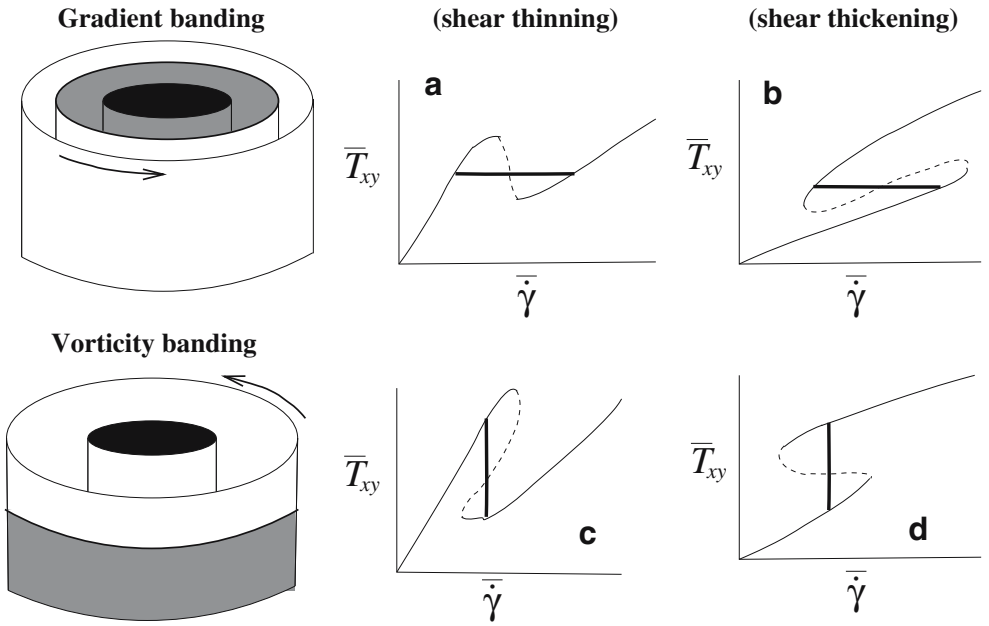


**Fig. 1** Candidate constitutive curves (*thin lines*) and shear rate $\dot{\gamma}$ or total stress $T_{xy}$ "plateaus" (*thick lines*) that could correspond to shear banding under either vorticity or gradient banding conditions. In all cases, the *dashed lines* are putative unstable steady flows that must be resolved into inhomogeneous shear banding states. The *overbars* signify that all quantities are the average values imposed by a rheometer. Homogeneous states could be observed for imposed conditions corresponding to the *thin solid lines*, while inhomogeneous shear-banding states could be observed for imposed conditions corresponding to the *thick solid lines*. As a few examples, rheological signatures consistent with **a** have been seen in wormlike micelle solutions (Cates and Fielding 2006), lyotropic lamellar surfactants (Diat et al. 1993), side-chain liquid crystal polymers (Pujolle-Robic and Noirez 2001), and many other systems. **b** has been seen in wormlike micelle solutions (Hu et al. 1998b). **c** has been seen in colloidal suspensions (Chen et al. 1992, 1994a, b), and **d** has been seen in lyotropic lamellar surfactant solutions (Diat et al. 1993; Bonn et al. 1998; Wilkins and Olmsted 2006)

transition from thickening to thinning occurs as a function of concentration, there is the intriguing possibility of seeing simultaneous vorticity and gradient banding, due to constitutive curves that resemble either Fig. 1b, or a superposition of both Fig. 1a and b. This may be the underlying root of very interesting time-dependent banding seen in Fischer et al. (2002).

Because wormlike micelles can undergo an isotropic-to-nematic phase transition, there is a possibility that the underlying constitutive curve can resemble that of Fig. 1c, where the underhanging branch is a nematic branch stabilized at high shear rates (Olmsted and Lu 1997, 1999a). Such a constitutive curve can in principle also support either vorticity or gradient banding; whether or not this is responsible for the curious mix of shear banding states reported in Britton and Callaghan (1999) remains an open question.

### Lamellar surfactant solutions

Roux and co-workers have uncovered an enormous number of interesting phenomena in lamellar surfactant solutions. Depending on the details of the composition, transitions can occur among lamellar states and multilamellar vesicles "onion" states (either disordered or in regular arrays), in which the onion state is thicker (Panizza et al. 1998; Roux et al. 1993; Diat et al. 1993). The transition is still not well-understood but is thought to be in part due to dilational pressures induced by inhomogeneous flows (due to defects in the lamellae or wall asperities), which induce a Helfrich–Hurault-like undulatory instability (Roux et al. 1993; Wunenburger et al. 2000; Zilman and Granek 1999; Marlow and Olmsted 2002). Some experimental evidence supports kinetic pathways of an instability of lamellae to cylinders (or "leeks"), which then convert to onions in steady state (Marlow and Olmsted 2002; Zipfel et al. 2001; Dhez et al. 2001; Le et al. 2001).

Once onions are formed, a variety of transitions similar to those seen in hard colloidal suspensions (liquid-like and crystal-like states) occur, with differences due to the softness of the onions: the onion size is a balance between shear and elastic forces, which can lead to a transition between states of different onion sizes (Panizza et al. 1998; Courbin et al. 2004). Onion transitions are very slow, probably due to the need for the onion size to adjust as a function of shear rate, which is a slow process that is largely unknown, but involves solvent permeation, defect motion and formation, and corresponding topological changes.

A number of interesting dynamical phenomena have been found in onions, including oscillations between liquid and crystalline onion order in nonsteady gradient banding configurations, as well as between onions of different sizes (Wunenburger et al. 2001; Courbin et al. 2004; Manneville et al. 2004b). This system has also yielded chaotic behavior (Salmon et al. 2002).

### Colloidal-like systems

A number of colloidal-like systems exhibit shear banding. Colloidal suspensions of hard spheres have been shown to exhibit vorticity banding between different degrees of crystalline order (Chen et al. 1992, 1994a, b). Block copolymer micelles in selective solvents (Eiser et al. 2000a, b) have been shown to also possess gradient banding transitions between different states of order, including an interested three-band coexistence of a disorder state and states of two layering orientations. Dense suspensions of soft particles exhibit banding signatures consistent with a solid-like jammed phase coexisting with a fluid phase: this has been seen in multiarm star polymers (Holmes et al. 2004a) in which a flowing liquid of stars seems to band together with a glassy stuck phase, and in dense monodisperse colloids subjected to large-amplitude oscillatory flow in a thin gap, in which a frozen solid crystal coexists with sliding layers (Cohen et al. 2004).

### Nematic liquid crystalline systems

Despite a number of theoretical studies (Edwards et al. 1991; Olmsted and Goldbart 1990, 1992; See et al. 1990) of shear banding phenomena in liquid crystals, there have been comparatively few experiments, probably because other phenomena deep in the nematic phase are very interesting in their own right, and the shear rates for inducing a transition are usually very high. However, gradient shear banding has been seen or inferred in lyotropic solutions (Mather et al. 1997) and in side-chain liquid crystalline melts (Pujolle-Robic and Noirez 2001). Recent studies of suspensions of rigid $fd$ virus suspensions, which are a good model for Onsager suspensions, demonstrated an extraordinary vorticity-banded structure, discussed elsewhere in this issue (Lettinga and Dhont 2004; Dhont et al. 2003; Kang et al. 2006). The structure comprises micron-sized bands of different director orientations stacked in the vorticity direction, which consist of similar morphologies of droplets in a matrix (either strongly nematic drops in a less nematic matrix or vice versa). Recent experiments suggest that this structure is roll-like, rather than the "canonical" vorticity banding suggested here (Kang et al. 2006).

### Polymer solutions

Shear thickening has been observed in dilute polymer solutions (Magda et al. 1993; Barham and Keller 1990; Kishbaugh and McHugh 1993), as well as oscillatory shear thickening behavior (Hilliou and Vlassopoulos 2002); see Larson (1992) for a review of related instabilities, some of which may involve shear banding.

The first microscopic model that predicted gradient banding was the Doi–Edwards (DE) theory for polymer melts. However, experiments have not supported this prediction, although there are a number of high-shear-rate instabilities related to wall effects (Boukany et al. 2006; Wang et al. 1996; Denn 2001). Hence, refined theories for polymer melts were developed based on convected constraint release (CCR) of entanglements (Marrucci 1996; Milner et al. 2001). In principle, polymer solutions should obey similar physics, with differences expected because of the coupling between stress and concentration fluctuations (Milner 1993; Imaeda et al. 2004; Fielding and Olmsted 2003b). More recently, a number of experiments of highly entangled semidilute solutions have shown signatures consistent with gradient banding (Tapadia et al. 2006; Tapadia and Wang 2006; Hu et al. 2007). Possible explanations for this behavior include: true gradient banding, a nearly flat stress plateau combined with the stress inhomogeneity inherent in rotating rheometers (Hu et al. 2007; Adams et al. 2007), a surface instability (Inn et al. 2005; Sui and McKenna 2007; Schweizer 2007), or melt fracture due to disentanglement (de Gennes 2007). This is a potentially fruitful area within which to further develop the understanding of entangled unbreakable polymer systems.

### Associating systems

Associating systems such as associating polymers and telechelic polymers also give rise to gradient banding, typically when the stress exceeds that necessary to extract the hydrophobes that form associative stickers; one example is a telechelic system in which the hydrophobes are incorporated into oil droplets (Berret and Séréro 2001; Michel et al. 2001), and another example is an associating polymer solution with a fraction of hydrophobe side chains (Annable et al. 1993).

## Steady states

The starting point in understanding shear banding is the steady banded state. This requires a theory for the high- and low-shear-rate branches and calculation of the inhomogeneous flow profile. The basic steps are outlined here.

### Formulation

The starting point for a theoretical description of banding is the momentum balance,

$$\rho\left(\partial_t + \mathbf{v}\cdot\nabla\right)\mathbf{v} = \nabla\cdot\boldsymbol{T}, \tag{1}$$

where $\boldsymbol{T}$ is the total stress tensor, $\rho$ is the density, and $\mathbf{v}$ is the fluid velocity. Most shear banding complex fluids occur in relatively slow flows at low Reynolds numbers, for which the creeping flow approximation is appropriate. Hence, the relation

$$\nabla\cdot\boldsymbol{T} = 0 \tag{2}$$

usually suffices. The total stress comprises a pressure $p$ to enforce incompressibility and a contribution from the microstructure, which is often separated into a Newtonian contribution and a viscoelastic contribution $\boldsymbol{\Sigma}$, as follows:

$$\boldsymbol{T} = \overset{\circ}{\boldsymbol{T}} - p\boldsymbol{I} \tag{3a}$$

$$= \boldsymbol{\Sigma} + 2\eta\boldsymbol{D} - p\boldsymbol{I}, \tag{3b}$$

where $\overset{\circ}{\boldsymbol{T}}$ is the traceless part of $\boldsymbol{T}$, $\boldsymbol{D} = \frac{1}{2}\left(\nabla\mathbf{v} + \nabla\mathbf{v}^T\right)$ is the symmetric velocity gradient tensor, and $\eta$ is a viscosity. Note that a division along the lines of Eq. 3b is often assumed, with an extra stress $\boldsymbol{\Sigma}$. This can sometimes lead to confusion because, in some cases, the "additional" microstructural stress $\boldsymbol{\Sigma}$ has a non-zero trace that contributes to the pressure.

The extra stress $\boldsymbol{\Sigma}$ has its own dynamics, which leads to a closed set of equations. This can either be in the form of an equation of motion for $\boldsymbol{\Sigma}$ or for other variables that $\boldsymbol{\Sigma}$ depends on. One example is the JS model, in which the form of Eq. 3b is assumed, with a differential equation of motion for the viscoelastic stress $\boldsymbol{\Sigma}$ (Johnson and Segalman 1977). Another example is the Doi model for liquid crystals, in which $\boldsymbol{\Sigma}$ is a function of the nematic order parameter $\boldsymbol{Q}$, which obeys a differential equation of motion (Olmsted and Lu 1999a; Doi 1981; Kuzuu and Doi 1983). A third model is Cates' reptation-reaction model for wormlike micelles, in which the viscoelastic stress is derived from its dependence on the molecular orientation and obeys an integral equation (Cates 1990).

Shear banding arises when the nonlinear coupling between flow and structure leads to multiple steady-state solutions to $\partial\boldsymbol{\Sigma}/\partial t = \mathbf{0}$, either for a given total shear stress $T_{xy}$ or for a given average shear rate $\dot{\gamma}$. These then lead to the underlying constitutive behavior, as in Fig. 1. Then, either gradient or vorticity banding

(or both) are possible, depending on the topology of the resulting constitutive curves.

## Gradient banding

### *Shear stress selection conditions*

We consider planar shear flow between plates, with unidirectional velocity $\mathbf{v} = \dot{\gamma}(y)\hat{\boldsymbol{x}}$. In a stereotypical shear banding flow, the total shear stress $T_{xy}$ has a multivalued *constitutive curve*, with stable flow branches $T^I_{xy}(\dot{\gamma})$ and $T^{II}_{xy}(\dot{\gamma})$ (e.g., Fig. 1a, b). We assume partitioning into two bands separated along the flow gradient direction, such that the only spatial variation is parallel to $\hat{\boldsymbol{y}}$. In planar unidirectional shear, the component $T_{zy}$ vanishes by symmetry. In the creeping flow equation, the other two components can then be integrated across the interface to yield

$$T^I_{xy}(\boldsymbol{\Sigma}, \dot{\gamma}) = T^{II}_{xy}(\boldsymbol{\Sigma}, \dot{\gamma}) = T^*_{xy} \tag{4a}$$

$$T^I_{yy}(\boldsymbol{\Sigma}, \dot{\gamma}) = T^{II}_{yy}(\boldsymbol{\Sigma}, \dot{\gamma}). \tag{4b}$$

The first equation implies a uniform shear stress, and the familiar result that the shear stress is the same in the two bands and equal to a constant, $T^*_{xy}$, the selected stress. Experimentally, the steady-state selected stress is usually observed to be independent of flow history and initial conditions.

This condition alone is not enough to resolve a unique shear stress, because there is typically a range of total shear stresses for which two shear rates are simultaneously locally stable. This resolution comes through the inclusion of nonlocal terms in the equations of motion for the microstructure, typically in the form of spatial gradient or "diffusion" terms (Olmsted and Lu 1997, 1999b; Olmsted and Goldbart 1990; Spenley et al. 1996; Dhont 1999),

$$\frac{\partial \boldsymbol{\Sigma}}{\partial t} = \boldsymbol{f}(\dot{\gamma}, \boldsymbol{\Sigma}) + \mathcal{D}\frac{\partial^2 \boldsymbol{\Sigma}}{\partial y^2} \tag{5}$$

where the nonlinear function $\boldsymbol{f}$ depends on the constitutive model (see Appendix for examples). Because the shear rate depends on $\boldsymbol{\Sigma}$ and the selected total shear stress $T^*_{xy}$ due to Eq. 4, Eq. 5 then yields a differential equation that determines the steady state profile $\boldsymbol{\Sigma}(y)$ for a given total shear stress $T_{xy}$.

The microstructure $\boldsymbol{\Sigma}$ must satisfy boundary conditions, such as $\hat{\boldsymbol{n}} \cdot \nabla \boldsymbol{\Sigma} = \mathbf{0}$ (Olmsted et al. 2000); although other choices such as specified values for $\boldsymbol{\Sigma}$ (Rossi 2006; Bhave et al. 1993; Cook and Rossi 2004) or mixed boundary conditions (Adams et al. 2007) are also possible (here, $\hat{\boldsymbol{n}}$ is the outward normal to the boundary). These boundary conditions are overspecified because both the value of the microstructure variable (to obtain the steady state stress on the constitutive curve) and the boundary condition must be simultaneously satisfied. In practice, these conditions become degenerate at a single total shear stress, which corresponds to the stress at which the interface between the two shear bands is stationary (Radulescu and Olmsted 2000).

The diffusion term(s) determines the interfacial width $\ell \sim \sqrt{\mathcal{D}}$. Note that this mechanism of stress selection, which is natural and relies on the presence of nonlocalities in the constitutive equations, obviates the need to define a nonequilibrium "free energy" to determine the selected stress, as has been suggested by some authors (Jou et al. 1995; Castillo-Tejas et al. 2005). Physical effects that can contribute to $\mathcal{D}$ include hydrodynamic interactions (Lu et al. 2000), particle diffusion (Bhave et al. 1993; El-Kareh and Leal 1989), and semiflexibility, which leads to the Frank elastic constants associated with liquid crystalline polymers (Liu and Fredrickson 1993).

In 1986, Krug suggested using diffusion terms to resolve the coexistence criterion in nonequilibrium phase transitions in driven diffusive lattice gases (Krug et al. 1986). In 1990, Frank elasticity, which penalizes spatial gradients, was used in models for liquid crystalline systems to provide unambiguous stress selection in shear banding around the isotropic–nematic transition (Olmsted and Goldbart 1990, 1992). Pearson realized in 1994 that the inherent history-dependence found in nonmonotonic constitutive curves could be resolved by introducing diffusion terms (Pearson 1994). In 1996, Spenley et al. introduced spatial gradients of the polymer shear stress in a scalar model for a nonmonotonic constitutive curve, to resolve stress selection and history-dependence (Spenley et al. 1996). Soon, spatial gradients were added to the JS model (Olmsted et al. 2000; Yuan 1999) in different forms (see the "*JS model*" section of the Appendix). In 1999, Dhont introduced a "curvature viscosity" to parameterize the contribution of gradients in shear rate to the total stress (Dhont 1999); predictions of this model are discussed elsewhere in this issue.

A general topological argument shows that, for nonmonotonic flow curves, any set of spatial gradient terms provide stress selection. That is, the total shear stress at which two shear states can coexist can occur either at isolated shear stresses or not at all (Lu et al. 2000). An equivalent description is in terms of the speed at which an interface between states moves. At the selected stress, the interface is stationary, while at other stresses, the interface moves (Radulescu and Olmsted 2000; Radulescu et al. 1999, 2003). Hence, stress selection is

a variant on the problem of the propagation of fronts, such as the front between two metastable states during a first-order phase transition (Kramer 1981).

*Nonuniqueness of stress selection*

If the constitutive equations have a single diffusion (spatial gradient) term, then the length scale of the system can be scaled out of the problem, and in an infinite system, the selected stress is independent of the magnitude of the diffusion term (Lu et al. 2000). Hence, a diffusion term is a singular perturbation to the dynamics, and any spatial gradients, no matter how small in magnitude, are enough to effect stress selection. However, the form of the diffusion term determines the selected stress. For example, the JS model has been calculated with two different forms for the diffusion coefficient:

$$\overset{\blacklozenge}{\boldsymbol{\Sigma}} + \frac{1}{\tau}\boldsymbol{\Sigma} = \begin{cases} 2\frac{\mu}{\tau}\boldsymbol{D} + \mathcal{D}\nabla^2\boldsymbol{\Sigma} & \text{(Olmsted et al. 2000)} \\ 2\frac{\mu}{\tau}\boldsymbol{D} - \mathcal{D}\nabla^2\boldsymbol{D}, & \text{(Yuan 1999)} \end{cases} \tag{6}$$

where the (Gordon–Schowalter) convected time derivative $\overset{\blacklozenge}{(\cdot)}$ is defined in the "*JS model*" section of the Appendix and $\mu$ is the "polymeric" viscosity. The constitutive curve is the same for both cases, given by

$$T_{xy} = \eta\dot{\gamma}\left[\varepsilon + \frac{1}{1+\dot{\gamma}^2\tau^2}\right], \tag{7}$$

where $\varepsilon = \eta/\mu$ is the viscosity ratio and $G = \mu/\tau$ is the characteristic modulus. The constitutive curve is nonmonotonic for $\varepsilon < 1/8$.

For the model with polymer stress diffusion, the selected stress must be calculated numerically. However, for the model in which shear rate diffusion is important, the selected stress can be calculated much more easily (Yuan 1999). The local shear rate determines the total shear stress according to

$$\frac{T_{xy}}{G} = \varepsilon\dot{\gamma}\tau + \frac{\dot{\gamma}\tau - \mathcal{D}\tau\frac{\partial^2\dot{\gamma}}{\partial y^2}}{1+\dot{\gamma}^2\tau^2}. \tag{8}$$

This can be integrated to give the following condition for the selected stress for a system of finite length $2L$.

$$\frac{T^*_{xy}}{G} = \frac{\left[\frac{1}{2}(1+\varepsilon)\hat{\dot{\gamma}}^2 + \frac{1}{4}\varepsilon\hat{\dot{\gamma}}^4 - \frac{1}{2}\mathcal{D}\left(\frac{\partial\hat{\dot{\gamma}}}{\partial y}\right)^2\right]_{-L}^{L}}{\left[\hat{\dot{\gamma}} + \frac{1}{3}\hat{\dot{\gamma}}^3\right]_{-L}^{L}}, \tag{9}$$

where the expressions in brackets are evaluated at either boundary of the system and $\hat{\dot{\gamma}} \equiv \dot{\gamma}\tau$ is the dimensionless shear rate. Using zero gradient boundary conditions and taking the infinite system limit, one finds the condition

$$\begin{aligned} \frac{T^*_{xy}}{G}&\left\{\hat{\dot{\gamma}}_1\left(T^*_{xy}\right) - \hat{\dot{\gamma}}_2\left(T^*_{xy}\right) + \frac{1}{3}\left[\hat{\dot{\gamma}}_1\left(T^*_{xy}\right) - \hat{\dot{\gamma}}_2\left(T^*_{xy}\right)\right]^3\right\} \\ &= \frac{1}{2}(1+\varepsilon)\left[\hat{\dot{\gamma}}_1\left(T^*_{xy}\right)^2 - \hat{\dot{\gamma}}_2\left(T^*_{xy}\right)^2\right] \\ &\quad + \frac{1}{4}\varepsilon\left[\hat{\dot{\gamma}}_1\left(T^*_{xy}\right)^4 - \hat{\dot{\gamma}}_2\left(T^*_{xy}\right)^4\right], \end{aligned} \tag{10}$$

where $\dot{\gamma}_1(T_{xy})$ and $\dot{\gamma}_2(T_{xy})$ are the shear rates on the stable low- and high-shear-rate branches of the constitutive curve. This condition can then be solved to find the selected stress. Figure 2 shows the selected stresses for the two constitutive models for different viscosity ratios $\varepsilon$. The selected stresses differ and are always independent of $\mathcal{D}$.

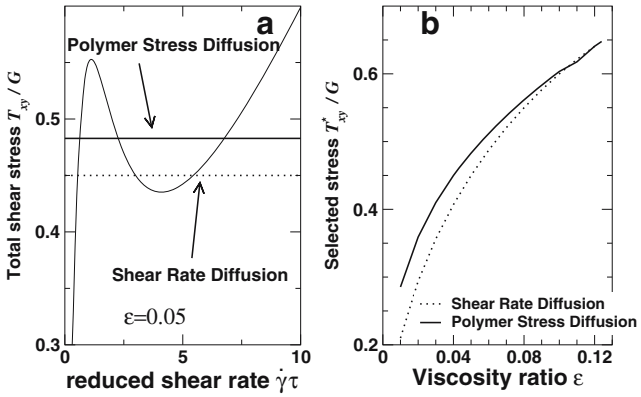


**Fig. 2** **a** Constitutive curves and selected stresses (*horizontal lines*) for the JS model with the spatial gradients (diffusion term) on either the shear rate or the polymer shear stress. **b** Selected stress as a function of viscosity ratio $\varepsilon$ for the two models

If a set of constitutive equations contains more than one spatial gradient term, which is the typical reality, only one of the corresponding coefficients can be scaled out of the system, leaving a dependence on the remaining ratios of coefficients. This was shown in a specific two-fluid model in which spatial gradients penalized both concentration and micellar stress inhomogeneities (Fielding and Olmsted 2003b).

*Normal stress balance conditions and instability*

Equation 4b above ensures equality of the normal force (stress) $T_{yy}$ across the interface. This can be separated into the pressure and a traceless contribution from the microstructure:

$$T_{yy} = \overset{\circ}{T}_{yy} - p, \tag{11}$$

so that continuity of the $yy$ component of stress leads to

$$\overset{\circ}{T}{}^{I}_{yy} - p_I = \overset{\circ}{T}{}^{II}_{yy} - p_{II}. \tag{12a}$$

The pressure will thus adjust, for unidirectional flow, to compensate for variations in the normal component of the microstructural stress. Variations in $p(y)$ do *not* give rise to flows in this case because the total stress is uniform. Hence, for example, pressure taps on either wall would give the same reading. However, the situation is different at the ends of the cell in the vorticity direction, $\hat{\boldsymbol{z}}$. At the top of the cell, for example, the normal stress in the $\hat{\boldsymbol{z}}$ direction will differ between the two phases:

$$T^I_{zz} - T^{II}_{zz} = N^{II}_2 - N^I_2, \tag{13}$$

using the definition of the second normal stress difference, $N_2 = T_{yy} - T_{zz}$, and making use of $T^I_{yy} = T^{II}_{yy}$.

This difference in normal stress $T_{zz}$ could be measured by a pressure tap in a closed cell. In an open cell, this stress is balanced against atmospheric pressure $p_0$ and any induced curvature in the meniscus:

$$T^{I,II}_{zz} = \overset{\circ}{T}{}^{I,II}_{zz} - p_{I,II} = -p_0 + \frac{\gamma_s}{R_{I,II}}, \tag{14}$$

where $\gamma_s$ is the air–fluid surface tension and a positive $R$ denotes curvature concave towards the fluid. For mechanical balance,

$$N^{II}_2 - N^I_2 = \gamma_s \left( \frac{1}{R_I} - \frac{1}{R_{II}} \right). \tag{15}$$

The three conditions, Eqs. 12a and 14, together with a constraint on the fixed total volume of fluid, determine the pressures $p_I$, $p_{II}$ and the curvature radii $R_I$, $R_{II}$ at the menisci. If these conditions cannot be satisfied then the shear banding fluid will become unstable. For large normal stress differences, one meniscus must be much more highly curved than the other, according to Eq. 15. For example, a large positive second normal stress difference in the shear-induced phase would require a small radius of curvature $R_{II}$. As the shear band grows due to an increasing average shear rate, this would eventually give rise to an instability because the small radius of curvature would be incompatible with a thick band. Hence, instability would occur as the plateau was traversed. This may be the source of some reported instabilities in wormlike micelle solutions. Some of these issues were noted by Lee et al. (2002) in the context of shear-thickening wormlike micelles.

## Vorticity banding

### Steady-state conditions

Vorticity banding, in which the inhomogeneity occurs along the vorticity direction, is more rare than gradient banding. The main reasons for this are that thickening is generally less prevalent than thinning (flow usually disrupts, instead of enhancing, structure); the kinetics are slower, as explained below; and first-order phase transitions, which will usually give rise to overhanging constitutive curves, occur at isolated points in phase space (Goveas and Olmsted 2001).

In an ideal flat plate geometry, bands which coexist along the vorticity direction $\hat{\boldsymbol{z}}$ must satisfy $\boldsymbol{T}^I \cdot \hat{\boldsymbol{z}} = \boldsymbol{T}^{II} \cdot \hat{\boldsymbol{z}}$. In steady state, each band is assumed to flow at the same uniform shear rate, with a velocity field $\mathbf{v} = \dot{\gamma} y \hat{\boldsymbol{x}}$. Hence, there is no shear at the interface between bands, so $T_{xz} = 0$. Moreover, $T_{yz} = 0$ everywhere because of symmetry. This leaves a final condition on the normal stress component,

$$T^I_{zz} = T^{II}_{zz}, \tag{16}$$

together with the condition that the shear rate be a constant independent of $z$ and thus the same in the two branches. Hence, one generally requires overhanging or underhanging constitutive curves (Fig. 3).

The steady state condition on the microstructure now becomes

$$0 = \boldsymbol{f}(\dot{\gamma}, \boldsymbol{\Sigma}) + \mathcal{D} \frac{\partial^2 \boldsymbol{\Sigma}}{\partial z^2}. \tag{17}$$

As with gradient banding, there is typically a range of shear rates that satisfy the balance conditions, as shown in Fig. 3. This degeneracy can again be resolved by solving Eq. 17, together with appropriate boundary conditions, to yield a selected strain rate $\dot{\gamma}^*$. This

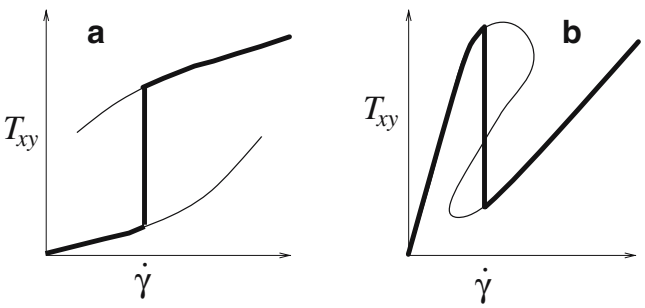


**Fig. 3** Constitutive curves that can support vorticity banding. **a** A shear thickening fluid. **b** A shear thinning fluid, possibly close to an equilibrium phase transition. In both cases, $\dot{\gamma}^*$ denotes a candidate selected strain rate, and the *thick curves* denote idealized flow curves that might be experimentally measured under controlled stress conditions

procedure was demonstrated in Olmsted and Lu (1997, 1999a). The resulting solution has two consequences for the measured pressures.

The first consequence is on the wall pressure distribution in the shear bands. For a given selected shear rate $\dot{\gamma}^*$, the microstructure on the two flow branches will have specific values far from the interfaces, $\mathbf{\Sigma}_I$, $\mathbf{\Sigma}_{II}$, given by $\boldsymbol{f}(\dot{\gamma}, \mathbf{\Sigma}) = 0$. Hence, the $zz$ component within a given shear band is given by

$$T_{zz}^{I,II} = \overset{\circ}{T}{}_{zz}^{I,II} - p_{I,II} = T_{zz}^*, \tag{18}$$

where the constant value $T_{zz}^*$ is determined by the selection condition. Because the microstructural stresses $\overset{\circ}{T}_{yy}$ in the two phases will generally differ, the pressures will adjust to maintain the same value for $T_{yy}$. Pressure taps on the side of the flow cell would measure the $yy$ component,

$$T_{yy}^{I,II} = \overset{\circ}{T}{}_{yy}^{I,II} - p_{I,II}. \tag{19}$$

These values would differ in the two phases. Eliminating the pressure difference using Eq. 18, one finds a difference in these values of

$$T_{yy}^I - T_{yy}^{II} = N_2^I - N_2^{II}. \tag{20}$$

Hence, the difference between measurements of pressure taps located in the two bands should equal the difference between the second normal stress differences of the two bands.

The second consequence is that of stability. As mentioned above, the value of the vertical component of stress $T_{zz}$ is determined by the selected shear rate. This must balance against the boundaries, in particular at the top of the shear cell. If the shear cell is closed, then the stress $T_{zz}^*$ would be measurable by a pressure tap. However, if the top of the cell is open, the vertical stress, which will generally be different from the ambient pressure due to the normal stresses in the fluid, must again be balanced by interfacial curvature; for example:

$$T_{zz}^* = -p_0 + \frac{\gamma_s}{R}. \tag{21}$$

As before, this condition may or may not be able to be satisfied depending on the size of the shear cell, and the system could thus become unstable.

## Experimental evidence for vorticity banding

Despite some theoretical work (Aradian and Cates 2005; Goveas and Olmsted 2001; Olmsted 1999; Olmsted and Lu 1999a) on vorticity banded systems, there has been very little systematic study of such systems. It has been observed in colloidal suspensions (Chen et al. 1992, 1994b), together with a rheological signal of a transition to a shear thinning phase, similar to Fig. 3b. The two phases corresponded to small polydomain (or liquid) and monodomain (or very large domain) colloidal crystals. There has been no subsequent work on this system. Diat et al. reported vorticity banding in the surfactant onion system, between bands of onion and non-onion lamellar phases, but did not perform a systematic study (Diat et al. 1993). Vorticity banding in a lamellar system was also reported in Bonn et al. (1998), but in that case, it was not clear whether or not the steady state of the system was vorticity or gradient banding. The same systems (SDS, dodecane, pentanol) was recently studied in a careful rheological study and found to have a rheological signature characteristic of vorticity banding, as in Fig. 3a, but it proved to be very difficult to observe macroscopic bands (Wilkins and Olmsted 2006).

The vorticity banding reported in the rigid-rod $fd$ virus suspension appears to be coupled to velocity rolls, and are thus not the uniform vorticity banding discussed here (Dhont et al. 2003; Kang et al. 2006; Lettinga and Dhont 2004). Similarly, oscillating vorticity banding was reported in a shear thickening wormlike micellar solution (Fischer et al. 2002; Wheeler et al. 1998), but not steady state vorticity banding.

There are several kinetic reasons for not seeing reproducible or clear vorticity banding. In a Couette cell, there is no stress gradient along the vorticity direction and, hence, no driving force to induce a new phase, unlike gradient banding, for which the stress gradient of cylindrical Couette flow provides a natural seed for shear banding (Greco and Ball 1997). Moreover, the stress gradients in cone-and-plate and Couette geometries provide a driving "force" to speed coarsening, whereas coarsening along the vorticity direction is purely unforced one-dimensional coarsening, which is known to be exponentially slow in time (Fife and McLeod 1977). Hence, not only is nucleation slower for vorticity banding, but the band structure is likely to consist of very fine bands that coarsen very slowly. One then must perform very long and patient experiments to see both a clear and reproducible rheological signature and macroscopically large (e.g., microns or larger) bands. Obviously, sedimentation will help if the bands have different concentrations and, thus, different densities. Another feature is that the interface in an ideal vorticity banding system is not under shear, unlike gradient banding, where the interface is experiencing shear. Shear is likely to provide extra fluctuations to aid nucleation-like events, as well as the growth of one phase into another.

## Models of shear banding

The Appendix collects a few models that exhibit shear banding, mainly for shear thinning fluids. The earliest rigorous analysis of unstable constitutive curves may have been in 1970 (Yerushalmi et al. 1970). This was followed by the introduction and analysis of the phenomenological JS model (Johnson and Segalman 1977; Malkus et al. 1990, 1991), and a study of the effect of flow on the nematic transition in liquid crystals (Hess 1976). The earliest microscopic model is probably the DE model for polymer melts (Doi and Edwards 1989), which can be cast as an integral equation for the extra elastic stress due the polymer. In this model, shear rates faster than the inverse reptation time induce an instability (McLeish and Ball 1986). Soon after this model was developed, the phenomenological JS model was introduced (Johnson and Segalman 1977), which is simpler and induces a nonmonotonic flow curve when the polymer stress fails to deform directly with the flow, but has "slip" according to the Gordon–Schowalter derivative (Malkus et al. 1991). The simplicity of this model has led to considerable use in theories of shear banding. Although the JS model by itself cannot predict the observed unique total shear stress selected during shear banding (Fyrillas et al. 1999; Georgiou 1998; Vlassopoulos and Hatzikiriakos 1995), with the addition of a diffusion term, the resulting diffusive JS (DJS) model is capable of describing shear banding (Olmsted et al. 2000; Yuan 1999).

The DE theory was extended by incorporating CCR of entanglements; the extra stress due to a sufficient rate of CCR, which allows other chains "snap" into the flow field, can render the constitutive curve monotonic. For small amounts of CCR, the model is unstable and predicts shear banding. A differential version of the model, the Rolie–Poly model, is reproduced in the Appendix (Eq. A15). A variant of this model can also be derived from Cates' model for wormlike micelles. Although the model has not been exhaustively studied, the nonmonotonic constitutive relation is arguably more physically motivated than the DJS model.

Manero et al. have developed a model in which the relaxation time for the extra stress itself depends on the shear rate (Castillo-Tejas et al. 2005; Escalante et al. 2003) and, hence, crudely captures the effects of flow on the micellar length, which is undoubtedly important.

An important degree of freedom is the concentration, which typically helps set the scale of the effective modulus of a particular system and controls the character of the self assembly. The intrinsic coupling between stress and concentration gradients, which has already been noted, has a destabilizing effect in shear flow (Milner 1993). Hence, two-fluid models, in which the extra stress is coupled to concentration, contain important physics. Schmitt et al. noted how concentration fluctuations couple to instabilities near shear banding transitions (Schmitt et al. 1995), and coupling to concentration is predicted to change a stress plateau to a finite-sloped plateau (Olmsted and Lu 1997; Olmsted 1999).

Concentration has thus been included in models for liquid crystalline suspensions (Olmsted and Lu 1997, 1999a) and in a two-fluid model that couples the DJS model to concentration (Fielding and Olmsted 2003a, b, c). This model captures some features of shear banding in wormlike micelles, such as an increasing banding stress with increasing concentration for systems far from the isotropic–nematic transition. A related two-fluid model has been derived by Cook et al. from a microscopic dumbbell approach that also uses the Gordon–Schowalter derivative of the DJS model (Cook and Rossi 2004; Rossi 2006).

An appealing system with relatively little experimental work is the isotropic–nematic transition. Theoretical studies of this system abound and only a few of the models are collected in the Appendix. Because of the proximity to a phase transition, there are underlying "overhanging" constitutive curves with the topology of Fig. 3b, which could support some combination of vorticity and gradient banding (Olmsted and Lu 1997, 1999a). There is a need to combine the physics of liquid crystalline ordering in flow with entanglement effects to describe semidilute or concentrated wormlike micellar solutions near the isotropic–nematic transition.

Many constitutive models for shear banding have included spatial gradient terms to describe interfacial structure and resolve stress selection. Such models lead to a smooth variation of the microstructure between shear bands. Although this is undoubtedly important and physically sensible, there are many systems in which the two phases are distinct and can hardly be expected to have a smooth transition between the coexisting states. One example is the lamellar-to-onion transition, in which a lamellar phase apparently coexists with an onion phase with a well-defined onion size; another is a shear thickening transition that induces a gel-like structure that coexists with a fluid, as occurs in shear thickening polymer solutions (Barham and Keller 1990), emulsions that yield so that a soft solid coexists with a fluid (Becu et al. 2005; Salmon et al. 2003a), or shear thickening wormlike micelle solutions (Hu et al. 1998a). Such systems would then need a separate interfacial constitutive relation to resolve stress selection; one candidate is a balance between rates of balances accretion and destruction of material at the interface, as

proposed by Ajdari (1998) and extended by Goveas and Pine (1999) to incorporate a stress-dependent reaction rate.

## Outstanding issues

The steady state phenomenology of shear banding is well-established, but many issues remain unclear. A microscopically faithful theoretical picture of the high-shear band state in wormlike micelles and polymer solutions does not yet exist. There has been little progress since the theory of Cates (1990) and related theories based on the tube model. The effects of features such as charge, polydisperse length distribution, micellar branching, cosurfactant concentration, and semiflexibility have barely been accounted for, even at a qualitative level. There is still very little understanding of the lamellar-to-onion shear banding transition. Although the role of spatial gradient (or "diffusion") terms is becoming clear, a clear microscopic foundation of these terms is lacking (but see Adams et al. 2007, for a recent discussion). Some systems with "overhanging" constitutive curves (as in Fig. 3) can support vorticity banding. Despite some speculation (Goveas and Olmsted 2001; Olmsted and Lu 1999a, b), we do not yet understand what determines which geometry (vorticity or gradient banding) obtains; candidates include kinetics, absolute stability, flow geometry, and flow history.

The most exciting new experiments have been those on dynamic and chaotic behavior in primarily wormlike micelles but also in other systems (lamellar surfactants, colloidal suspensions). After shear banding was established, it was realized that very long transients often accompany the establishment of steady state. Experiments under controlled stress or controlled strain rate give results analogous to the kinetics of phase ordering in first-order phase transitions, such as delayed growth, unstable growth, induction times, and the like (Berret 1997; Berret and Porte 1999; Grand et al. 1997). Spatial diffusion terms play a role in this, and experiments on transients after strain rate jumps have been used to estimate the magnitude of the diffusion term (Radulescu et al. 2003).

A number of experiments have been interpreted in terms of chaotic or rheo-chaotic signatures, including wormlike micelles (Bandyopadhyay et al. 2000; Ganapathy and Sood 2006a, b; Ganapathy et al. 2007; Sood et al. 1999) and lamellar surfactant systems (Manneville et al. 2004b; Salmon et al. 2002). These experiments have spawned a number of theoretical studies of simple local (Cates 2002; Head et al. 2002) and nonlocal models (Aradian and Cates 2005; Fielding and Olmsted 2004) for shear banding. Slightly more realistic models based on tensorial liquid crystalline models have uncovered a host of other spatiotemporal behaviors (Chakrabarti et al. 2004; Das et al. 2005; Forest et al. 2004; Rienacker et al. 2002a, b) However, it is fair to say that the models remain far from the experiments, and a credible microscopic model for the complex dynamical behavior is still lacking.

Other complex behavior has included more detailed measurements of band wandering and interface fluctuations in wormlike micelles, using both ultrasound (Bécu et al. 2007; Becu et al. 2004) and NMR (Holmes et al. 2003; Lopez-Gonzalez et al. 2004). Recent experiments have shown fascinating instabilities at the interface between the two shear bands in wormlike micelles, including undulations and nonlinear waves in the vorticity direction (Decruppe et al. 2006; Lerouge et al. 2006). The occurrence of this in a solution featuring the well-studied cetyltrimethylammonium bromide surfactant suggests that such behavior may be more common than previously suspected.

Two recent studies of the DJS model have shown that the interface is unstable to two-dimensional fluctuations (Fielding 2005; Wilson and Fielding 2006). Although the instability can in some cases be weakly stabilized by nonlinear fluctuations (Fielding and Olmsted 2006), this is only for unphysically large interface widths $\ell$. Hence, the DJS model may not be the most appropriate model for studying stable one-dimensional shear banding. Conversely, the increasing ubiquity of complex spatiotemporal behavior observed in micellar systems may be consistent with this model! Nonetheless, it is important to determine whether or not this instability, whose source can be traced to normal stress differences across the interface (McLeish 1987), is present in other models.

Another area of promise is the interplay between constitutive instabilities and boundary conditions. Wall slip seems to play a role or at least occurs simultaneously with shear banding in some cases (Becu et al. 2004, 2005; Manneville et al. 2007), and interaction with the wall asperities has been thought to influence the formation of onions in lamellar surfactant solutions.

## Conclusion

I have presented a short review of some of the outstanding issues in shear banding and given a pedagogical account of the steady state conditions and their implications for stability in both vorticity and gradient banded configurations. A careful study of the stress balances shows that free surfaces should be curved due to normal

stress differences between the two states. Sufficiently strong normal stresses could lead to an instability at the free surface. In gradient banding states, the normal stresses in the high-shear-rate phase should induce a curved interface, which could become unstable when the shear band grows too wide so support a highly curved interface.

I have shown, using variants of the DJS model, how different diffusion terms give rise to different values of the total shear stress on the stress plateau. Although diffusion terms are acknowledged to determine spatial structure, we lack a firm microscopic picture of their source and magnitude in systems as well studied as wormlike micelles. These terms will undoubtedly take on more importance as the body of experimental measurements of spatio-temporal structure in shear banding systems increases.

**Acknowledgements** I thank David Lu, Simon Marlow, Ovidiu Radulescu, Georgina Wilkins, James Adams, and especially Suzanne Fielding for enjoyable and fruitful collaborations and a host of the experimental shear banding community for continual inspiration; much of this work was supported by the Engineering and Physical Sciences Research Council (UK).

## Appendix

Models that exhibit shear banding

*JS model*

In the JS model, the total stress is assumed to be divided as in Eq. 3b, and the viscoelastic stress $\boldsymbol{\Sigma}$ is assumed to obey (Johnson and Segalman 1977; Olmsted et al. 2000)

$$\overset{\blacklozenge}{\boldsymbol{\Sigma}} + \frac{1}{\tau}\boldsymbol{\Sigma} = 2\frac{\mu}{\tau}\boldsymbol{D} + \mathcal{D}\nabla^2\boldsymbol{\Sigma}, \tag{A1}$$

where

$$\overset{\blacklozenge}{\boldsymbol{\Sigma}} = (\partial_t + \mathbf{v}\cdot\nabla)\boldsymbol{\Sigma} + (\boldsymbol{\Omega}\boldsymbol{\Sigma} - \boldsymbol{\Sigma}\boldsymbol{\Omega}) - a(\boldsymbol{D}\boldsymbol{\Sigma} + \boldsymbol{\Sigma}\boldsymbol{D}) \tag{A2}$$

is the Gordon–Schowalter derivative (Larson 1988), $\tau$ is a relaxation time, the "polymer" viscosity $\mu$ determines a modulus $G = \mu/\tau$, and $\boldsymbol{\Omega} = \frac{1}{2}\left[\nabla\mathbf{v} - (\nabla\mathbf{v})^T\right]$. The total stress comprises the viscoelastic stress of the DJS model and a Newtonian contribution, according to Eq. 3b, and the viscosity ratio $\epsilon \equiv \eta/\mu$ controls the balance between the two stresses. The "slip parameter" $a$, which describes nonaffine stretch of the dumbbell with respect to the extension of the flow, allows for a nonmonotonic constitutive curve for $0 < |a| < 1$ and $\epsilon < 1/8$.

The "diffusion" term $\mathcal{D}\nabla^2\boldsymbol{\Sigma}$ describes nonlocal relaxation of the viscoelastic stress and is necessary to describe strongly inhomogeneous flow profiles (Olmsted et al. 2000). Because of this term, the steady shear banding state obeys a spatial differential equation, which must be solved subject to boundary conditions specified at the walls of the flow cell. The solvability condition for a stationary interface leads to a unique total shear stress plateau for imposed average shear rates in the nonmonotonic portion of the constitutive curve (Lu et al. 2000). The characteristic width $\ell$ of the interface between shear bands is given by $\ell = \sqrt{\mathcal{D}\tau}$.

Yuan has proposed an alternative form for a diffusion term, which is similar to the "curvature viscosity" term proposed by Dhont (1999). In this version, spatial gradients in the local shear rate contribute to stress relaxation (Yuan 1999)

$$\overset{\blacklozenge}{\boldsymbol{\Sigma}} + \frac{1}{\tau}\boldsymbol{\Sigma} = 2\frac{\mu}{\tau}\boldsymbol{D} - \mathcal{D}\nabla^2\boldsymbol{D}. \tag{A3}$$

The DJS model has been coupled to concentration degrees of freedom in several different guises (Cook and Rossi 2004; Fielding and Olmsted 2003a, b, c; Rossi 2006; Yuan and Jupp 2002).

*Liquid crystal hydrodynamics*

A suspension of long rigid rods undergoes an isotropic-to-nematic phase transition at a sufficiently high concentration. Flow can induce the nematic phase, and the dynamical equations of motion support shear banding. In this case, the microstructural stress is a function of the nematic order parameter tensor $\boldsymbol{Q} = \langle\hat{\boldsymbol{u}}\hat{\boldsymbol{u}}\rangle - \frac{1}{3}\boldsymbol{I}$, where the unit vector $\hat{\boldsymbol{u}}$ denotes the orientation of a rigid rod. There have been many essentially equivalent independent derivations of the hydrodynamic equations of motion, both phenomenologically and from a molecular point of view. Perhaps the most precise derivation is the recent one of Stark and Lubensky (2003), based on microscopic Poisson Brackets. The general form is as follows (Doi 1981; Edwards et al. 1990; Hess 1975; Kuzuu and Doi 1983; Olmsted and Goldbart 1990):

$$\overset{\bullet}{\boldsymbol{Q}} = \frac{1}{\zeta_Q}\,\overset{\circ}{\boldsymbol{H}}(\boldsymbol{Q}) + \boldsymbol{\Lambda} : \boldsymbol{D}, \tag{A4}$$

where

$$\overset{\bullet}{\boldsymbol{Q}} = (\partial_t + \mathbf{v}\cdot\nabla)\boldsymbol{Q} + (\boldsymbol{\Omega}\boldsymbol{Q} - \boldsymbol{Q}\boldsymbol{\Omega}) \tag{A5}$$

is the corotational derivative and $\zeta_Q$ is a relaxation coefficient. The reactive fourth rank tensor $\boldsymbol{\Lambda}$ describes

nondissipative evolution of the order parameter tensor. The molecular field that drives relaxation to equilibrium is

$$\boldsymbol{H} = -\frac{\delta \mathcal{F}}{\delta \boldsymbol{Q}}, \tag{A6}$$

where the free energy functional $\mathcal{F}$ includes homogeneous and inhomogeneous (Frank elastic) terms. The stress has a viscous part $\boldsymbol{T}^v$, a symmetric elastic part $\boldsymbol{T}^{el}$, and an antisymmetric part $\boldsymbol{T}^a$, as follows:

$$\boldsymbol{T} = \boldsymbol{T}^v + \boldsymbol{T}^{el} + \boldsymbol{T}^a - p\boldsymbol{I} \tag{A7}$$

$$\boldsymbol{T}^v = \boldsymbol{\eta} : \boldsymbol{D} \tag{A8}$$

$$\boldsymbol{T}^a = \boldsymbol{H}\boldsymbol{Q} - \boldsymbol{Q}\boldsymbol{H} \tag{A9}$$

$$\boldsymbol{T}^{el} = -\boldsymbol{\Lambda} : \overset{\circ}{\boldsymbol{H}} - \nabla Q_{\alpha\beta} \cdot \frac{\delta \mathcal{F}}{\delta \nabla Q_{\alpha\beta}}, \tag{A10}$$

where $\boldsymbol{\eta}$ is a fourth rank viscosity tensor that generally depends on $\boldsymbol{Q}$, and the term $-\boldsymbol{\Lambda} : \overset{\circ}{\boldsymbol{H}}$ ensures Onsager reciprocity. Recall that $\overset{\circ}{\boldsymbol{H}}$ is the traceless-symmetric version of $\boldsymbol{H}$. The elastic stress is equivalent to the elastic stress due to Frank elasticity (de Gennes and Prost 1993), generalized to a description in terms of the nematic order parameter $\boldsymbol{Q}$ rather than the nematic director. The free energy $\mathcal{F}(\boldsymbol{Q})$ describes the isotropic–nematic phase transition, and the coupling to flow $\boldsymbol{\Lambda} : \boldsymbol{D}$ in Eq. A4 perturbs the isotropic state and induces a phase transition. The choice of $\boldsymbol{\Lambda}$ is somewhat a matter of taste and has been derived from a microscopic picture by Doi et al. and by Stark and Lubensky (Doi 1981; Edwards et al. 1990; Hess 1975; Kuzuu and Doi 1983; Olmsted and Goldbart 1990; Stark and Lubensky 2003).

The simple choice $\boldsymbol{\Lambda} : \boldsymbol{D} = \nu \boldsymbol{D}$ was chosen in an early study of the effects of flow on the isotropic–nematic phase transition (Olmsted and Goldbart 1990, 1992). From a microscopic model, Stark and Lubensky derived the following:

$$\boldsymbol{\Lambda} : \boldsymbol{D} = (\boldsymbol{D}\boldsymbol{Q} + \boldsymbol{Q}\boldsymbol{D}) + \frac{I}{3\Delta I}\boldsymbol{D} \tag{A11}$$

$$- 2\left[\frac{1}{3}\boldsymbol{I} + \left(1 + \frac{I}{\Delta I}\right)\boldsymbol{Q}\right] \mathrm{Tr}(\boldsymbol{Q}\boldsymbol{D}), \tag{A12}$$

where $I$ is the principal moment of inertia and $\Delta I$ the difference between the two moments of inertia of uniaxial rods. In the Doi model $\boldsymbol{\Lambda}$ is defined by

$$\boldsymbol{\Lambda} : \boldsymbol{D} = (\boldsymbol{D}\boldsymbol{Q} + \boldsymbol{Q}\boldsymbol{D}) + \frac{2}{3}\boldsymbol{D} - 2\left(\boldsymbol{Q} + \frac{1}{3}\boldsymbol{I}\right) \mathrm{Tr}(\boldsymbol{Q}\boldsymbol{D}). \tag{A13}$$

This model was coupled to concentration to explore the effects of shear flow on the isotropic–nematic phase transition in suspensions (Olmsted and Lu 1997, 1999a). In the Beris–Edwards model, the same choice is made with an additional prefactor $\xi$ that can be related to the aspect ratio of the rigid rods (Edwards et al. 1990; Kuzuu and Doi 1983) and is essentially the same as the slip parameter $a$ that appears in the Gordon–Schowalter derivative; this was used by Denniston and Yeomans in a lattice Boltzmann study (Denniston et al. 2001). Hess and Kröger used the choice (Rienacker et al. 2002a)

$$\boldsymbol{\Lambda} : \boldsymbol{D} = a\left[\boldsymbol{D}\boldsymbol{Q} + \boldsymbol{Q}\boldsymbol{D} - \frac{2}{3}\boldsymbol{I}\mathrm{Tr}(\boldsymbol{Q}\boldsymbol{D})\right] + \alpha \boldsymbol{D} \tag{A14}$$

in their study of chaotic dynamics in nematic liquid crystals, where $\alpha$ was related to a ratio of Leslie–Erickson coefficients. A similar choice was made in another study of chaotic dynamics (Das et al. 2005). Other microscopically derived constitutive equations include those of Dhont and Briels (2003a, b) and of Calderer et al. (2004); the former is notable for its incorporation of inhomogeneous flows.

*Rolie–Poly model*

The original DE theory for entangled polymer dynamics predicted a nonmonotonic constitutive curve and an instability that could lead to shear banding (Doi and Edwards 1989; McLeish 1987; McLeish and Ball 1986). This early pioneering model neglected an important physical source of stress under flow, which has been recently understood and modeled: the enhanced release of polymer entanglements due to convection (Marrucci 1996). This increases the polymer stress and, for sufficiently strong convected constraint release (CCR), can "cure" the DE instability. CCR and tube stretching were incorporated in Milner et al. (2001) to describe polymer melts and wormlike micelles and later simplified to the following differential version, called the Rolie–Poly model (Likhtman and Graham 2003):

$$\overset{\blacktriangledown}{\boldsymbol{\Sigma}} + \frac{1}{\tau}\boldsymbol{\Sigma} = 2G\boldsymbol{D} - \frac{2}{3}\boldsymbol{\Sigma} : \nabla \mathbf{v}\left[\boldsymbol{I} + (1+\beta)\frac{\boldsymbol{\Sigma}}{G}\right] + \mathcal{D}\nabla^2\boldsymbol{\Sigma}. \tag{A15}$$

The CCR parameter $\beta$ $(0 \le \beta \le 1)$ is proportional to the frequency of the release of polymer entanglement constraints due to convection by the flow. Likhtman and Graham (2003) used $\beta = 1$ to model a well-entangled polymer melt without a constitutive instability. For small enough $\beta$, a constitutive instability results, akin to the original DE instability (Adams et al. 2007). The stress diffusion included above did not appear in the original formulation. In the version of the

Rolie–Poly model used in Eq. A15, the tube length is assumed to be relaxed ("nonstretching").

Interestingly, the limit $\beta = 0$ corresponds to a differential version of the Cates model (Cates 1990) of wormlike micellar solutions. This constitutive equation can be obtained by rewriting the original integral equation as a differential equation and then using a decoupling approximation to remove fourth-order moments (Adams et al. 2007; McLeish 1997).

## References


Adams JM, Olmsted PD, Fielding SM (2007) The interplay between boundary conditions and flow geometries in shear banding: hysteresis, band configurations, and surface transitions. http://arxiv.org/abs/0710.3242v1

Ajdari A (1998) Rheological behavior of a solution of particles aggregating on the containing walls. Phys Rev E 58: 6294–6297

Annable T, Buscall R, Ettelaie R, Whittlestone D (1993) The rheology of solutions of associating polymers: comparison of experimental behavior with transient network theory. J Rheol 37:695

Aradian A, Cates ME (2005) Instability and spatiotemporal rheochaos in a shear-thickening fluid model. Europhys Lett 70:397–403

Bandyopadhyay R, Basappa G, Sood AK (2000) Observation of chaotic dynamics in dilute sheared aqueous solutions of CTAT. Phys Rev Lett 84:2022–2025

Barentin C, Liu AJ (2001) Shear thickening in dilute solutions of wormlike micelles. Europhys Lett 55:432–438

Barham PJ, Keller A (1990) Flow-induced liquid-liquid phase separation and adsorption entanglement layer formation in high-molecular-weight polymer solutions. Macromolecules 23:303–309

Becu L, Manneville S, Colin A (2004) Spatiotemporal dynamics of wormlike micelles under shear. Phys Rev Lett 93:018301

Becu L, Grondin P, Colin A, Manneville S (2005) How does a concentrated emulsion flow? Yielding, local rheology, and wall slip. Colloid Surf A-Physicochem Eng Asp 263:146–152

Bécu L, Anache D, Manneville S, Colin A (2007) Evidence for three-dimensional unstable flows in shear-banding wormlike micelles. Phys Rev E 76:011503

Bergenholtz J, Wagner NJ (1996) Formation of AOT/brine multilamellar vesicles. Langmuir 12:3122–3126

Berret JF (1997) Transient rheology of wormlike micelles. Langmuir 13:2227–2234

Berret J-F (2005) Molecular gels. In: Weiss RG, Terech P (eds) Chap. Rheology of wormlike micelles: equilibrium properties and shear banding transition. Springer, Dordrecht, pp 235–275

Berret JF, Porte G (1999) Metastable versus unstable transients at the onset of a shear-induced phase transition. Phys Rev E 60:4268–4271

Berret J, Séréro Y (2001) Evidence of shear-induced fluid fracture in telechelic polymer networks. Phys Rev Lett 87:48303

Berret JF, Roux DC, Porte G, Lindner P (1994) Shear-induced isotropic-to-nematic phase-transition in equilibrium polymers. Europhys Lett 25:521–526

Berret JF, Porte G, Decruppe JP (1997) Inhomogeneous shear flows of wormlike micelles: a master dynamic phase diagram. Phys Rev E 55:1668–1676

Berret JF, Gamez-Corrales R, Oberdisse J, Walker LM, Lindner P (1998) Flow-structure relationship of shear-thickening surfactant solutions. Europhys Lett 41:677–682

Bhave AV, Menon RK, Armstrong RC, Brown RA (1993) A constitutive equation for liquid-crystalline polymer solutions. J Rheol 37:413–441

Boltenhagen P, Hu YT, Matthys EF, Pine DJ (1997) Observation of bulk phase separation and coexistence in a sheared micellar solution. Phys Rev Lett 79:2359–2362

Bonn D, Meunier J, Greffier O, Alkahwaji A, Kellay H (1998) Bistability in non-Newtonian flow: rheology of lyotropic liquid crystals. Phys Rev E 58:2115–2118

Boukany PE, Tapadia P, Wang SQ (2006) Interfacial stick-slip transition in simple shear of entangled melts. J Rheol 50: 641–654

Britton MM, Callaghan PT (1999) Shear banding instability in wormlike micellar solutions. Eur Phys J B 7:237–249

Bruinsma R, Gelbart WM, Benshaul A (1992) Flow-induced gelation of living (micellar) polymers. J Chem Phys 96: 7710–7727

Calderer MC, Forest MG, Wang Q (2004) Kinetic theories and mesoscopic models for solutions of nonhomogeneous liquid crystal polymers. J Non-Newton Fluid Mech 120:69–78

Callaghan PT, Cates ME, Rofe CJ, Smeulders JAF (1996) A study of the spurt effect in wormlike micelles using nuclear-magnetic-resonance microscopy. J Phys II 6:375–393 (France)

Cappelaere E, Berret JF, Decruppe JP, Cressely R, Lindner P (1997) Rheology, birefringence, and small-angle neutron scattering in a charged micellar system: evidence of a shear-induced phase transition. Phys Rev E 56:1869–1878

Castillo-Tejas J, Alvarado JFJ, Gonzalez-Alatorre G, Luna-Barcenas G, Sanchez IC, Macias-Salinas R, Manero O (2005) Nonequilibrium molecular dynamics of the rheological and structural properties of linear and branched molecules. Simple shear and poiseuille flows; instabilities and slip. J Chem Phys 123:054907

Cates ME (1990) Nonlinear viscoelasticity of wormlike micelles (and other reversibly breakable polymers). J Phys Chem 94:371–375

Cates M, Candau S (1990) Statics and dynamics of worm-like surfactant micelles. J Phys Condens Matter 2:6869–6892

Cates ME, Candau SJ (2001) Ring-driven shear thickening in wormlike micelles? Europhys Lett 55:887–983

Cates ME, Fielding SM (2006) Rheology of giant micelles. Adv Phys 55:799–879

Cates ME, Turner MS (1990) Flow-induced gelation of rodlike micelles. Europhys Lett 11:681–686

Cates ME, Head DA, Ajdari A (2002) Rheological chaos in a scalar shear-thickening model. Phys Rev E 66:025202

Chakrabarti B, Das M, Dasgupta C, Ramaswamy S, Sood AK (2004) Spatiotemporal rheochaos in nematic hydrodynamics. Phys Rev Lett 92:055501

Chen LB, Zukoski CF, Ackerson BJ, Hanley HJM, Straty GC, Barker J, Glinka CJ (1992) Structural-changes and orientational order in a sheared colloidal suspension. Phys Rev Lett 69:688–691

Chen LB, Ackerson BJ, Zukoski CF (1994a) Rheological consequences of microstructural transitions in colloidal crystals. J Rheol 38:193–216

Chen LB, Chow MK, Ackerson BJ, Zukoski CF (1994b) Rheological and microstructural transitions in colloidal crystals. Langmuir 10:2817–2829

Cohen I, Mason TG, Weitz DA (2004) Shear-induced configurations of confined colloidal suspensions. Phys Rev Lett 93:46001

Cook LP, Rossi LR (2004) Slippage and migration in models of dilute wormlike micellar solutions and polymeric fluids. J Non-Newton Fluid Mech 116:347–369
Courbin L, Panizza P, Salmon JB (2004) Observation of droplet size oscillations in a two-phase fluid under shear flow. Phys Rev Lett 92:018305
Das M, Chakrabarti B, Dasgupta C, Ramaswamy S, Sood AK (2005) Routes to spatiotemporal chaos in the rheology of nematogenic fluids. Phys Rev E 71:021707
Decruppe JP, Cressely R, Makhloufi R, Cappelaere E (1995) Flow birefringence experiments showing a shear-banding structure in a CTAB solution. Coll Polym Sci 273:346–351
Decruppe JP, Greffier O, Manneville S, Lerouge S (2006) Local velocity measurements in heterogeneous and time-dependent flows of a micellar solution. Phys Rev E 73: 061509
de Gennes PG (2007) Melt fracture of entangled polymers. Eur Phys J E 23:3–5
de Gennes PG, Prost J (1993) The physics of liquid crystals, 2nd edn. Clarendon, Oxford
Denn MM (2001) Extrusion instabilities and wall slip. Annu Rev Fluid Mech 33:265–287
Denniston C, Orlandini E, Yeomans JM (2001) Lattice Boltzmann simulations of liquid crystal hydrodynamics. Phys Rev E 63:56702
Dhez O, Nallet F, Diat O (2001) Influence of screw dislocations on the orientation of a sheared lamellar phase. Europhys Lett 55:821–826
Dhont JKG (1999) A constitutive relation describing the shear-banding transition. Phys Rev E 60:4534–4544
Dhont JKG, Briels WJ (2003a) Inhomogeneous suspensions of rigid rods in flow. J Chem Phys 118:1466–1478
Dhont JKG, Briels WJ (2003b) Viscoelasticity of suspensions of long, rigid rods. Colloid Surf A Physicochem Eng Asp 213:131–156
Dhont JKG et al (2003) Shear-banding and microstructure of colloids in shear flow. Faraday Discuss 123:157–172
Diat O, Roux D, Nallet F (1993) Effect of shear on a lyotropic lamellar phase. J Phys II 3:1427–1452 (France)
Doi M (1981) Molecular dynamics and rheological properties of concentrated solutions of rodlike polymers in isotropic and liquid crystalline phases. J Poly Sci Poly Phys 19:229–243
Doi M, Edwards SF (1989) The theory of polymer dynamics. Clarendon, Oxford
Edwards BJ, Beris AN, Grmela M, Larson RG (1990) Generalized constitutive equation for polymeric liquid-crystals. 2. Nonhomogeneous systems. J Non-Newton Fluid Mech 36:243–254
Edwards BJ, Beris AN, Grmela M (1991) The dynamic behavior of liquid-crystals—a continuum description through generalized brackets. Mol Cryst Liq Cryst 201:51–86
Eiser E, Molino F, Porte G, Diat O (2000a) Nonhomogeneous textures and banded flow in a soft cubic phase under shear. Phys Rev E 61:6759–6764
Eiser E, Molino F, Porte G, Pithon X (2000b) Flow in micellar cubic crystals. Rheol Acta 39:201–208
El-Kareh AW, Leal LG (1989) Existence of solutions for all Deborah numbers for a non-Newtonian model modified to include diffusion. J Non-Newton Fluid Mech 33: 257–287
Escalante J, Macias E, Bautista F, Pérez-López J, Soltero J, Puig J, Manero O (2003) Shear-banded flow and transient rheology of cationic wormlike micellar solutions. Langmuir 19:6620–6626
Fielding SM (2005) Linear instability of planar shear banded flow. Phys Rev Lett 95:134501
Fielding SM (2007) Complex dynamics of shear banded flows. Soft Matter 3:1262–1279
Fielding SM, Olmsted PD (2003a) Early stage kinetics in a unified model of shear-induced demixing and mechanical shear banding instabilities. Phys Rev Lett 90:224501
Fielding SM, Olmsted PD (2003b) Flow phase diagrams for concentration-coupled shear banding. Eur Phys J E 11: 65–83
Fielding SM, Olmsted PD (2003c) Kinetics of the shear banding instability in startup flows. Phys Rev E 68:036313
Fielding SM, Olmsted PD (2004) Spatiotemporal oscillations and rheochaos in a simple model of shear banding. Phys Rev Lett 92:084502
Fielding SM, Olmsted PD (2006) Nonlinear dynamics of an interface between shear bands. Phys Rev Lett 96:104502
Fife PC, McLeod JB (1977) The approach of solutions of nonlinear diffusion equations to travelling front solutions. Arch Rat Mech Anal 65:335–361
Fischer P, Wheeler EK, Fuller GG (2002) Shear-banding structure orientated in the vorticity direction observed for equimolar micellar solution. Rheol Acta 41:35–44
Forest MG, Zhou RH, Wang Q (2004) Chaotic boundaries of nematic polymers in mixed shear and extensional flows. Phys Rev Lett 93:088301
Fyrillas MM, Georgiou GC, Vlassopoulos D (1999) Time-dependent plane poiseuille flow of a Johnson-Segalman fluid. J Non-Newton Fluid Mech 82:105–123
Gamez-Corrales R, Berret JF, Walker LM, Oberdisse J (1999) Shear-thickening dilute surfactant solutions: equilibrium structure as studied by small-angle neutron scattering. Langmuir 15:6755–6763
Ganapathy R, Sood AK (2006a) Intermittency route to rheochaos in wormlike micelles with flow-concentration coupling. Phys Rev Lett 96:108301
Ganapathy R, Sood AK (2006b) Tuning rheochaos by temperature in wormlike micelles. Langmuir 22:11016–11021
Ganapathy R, Rangarajan G, Sood AK (2007) Granger causality and cross recurrence plots in rheochaos. Phys Rev E 75:16211
Georgiou GC, Vlassopoulos D (1998) On the stability of the simple shear flow of a Johnson–Segalman fluid. J Non-Newton Fluid Mech 75:77–97
Goveas JL, Olmsted PD (2001) A minimal model for vorticity and gradient banding in complex fluids. Eur Phys J E6: 79–89
Goveas JL, Pine DJ (1999) A phenomenological model for shear-thickening in wormlike micelle solutions. Europhys Lett 48:706–706
Grand C, Arrault J, Cates ME (1997) Slow transients and metastability in wormlike micelle rheology. J Phys II 7: 1071–1086 (France)
Greco F, Ball RC (1997) Shear-band formation in a non-Newtonian fluid model with a constitutive instability. J Non-Newton Fluid Mech 69:195–206
Head DA, Ajdari A, and Cates ME (2002) Rheological instability in a simple shear-thickening model. Europhys Lett 57: 120–126
Herle V, Fischer P, Pfister B, Kohlbrecher J, Windhab EJ (2005) Structural characterization of shear banded flow in shear thickening wormlike micellar system. Langmuir 21:9051
Hess S (1975) Irreversible thermodynamics of nonequilibrium alignment phenomena in molecular liquids and in liquid crystals. Z Naturforsch 30a:728–733
Hess S (1976) Pre- and post-transitional behavior of the flow alignment and flow-induced phase transition in liquid crystals. Z Naturforsch 31a:1507

Hilliou L, Vlassopoulos D (2002) Time-periodic structures and instabilities in shear-thickening polymer solutions. Ind Eng Chem Res 41:6246–6255

Holmes WM, Lopez-Gonzalez MR, Callaghan PT (2003) Fluctuations in shear-banded flow seen by NMR velocimetry. Europhys Lett 64:274–280

Holmes WM, Callaghan PT, Vlassopoulos D, Roovers J (2004a) Shear banding phenomena in ultrasoft colloidal glasses. J Rheol 48:1085–1102

Holmes WM, Lopez-Gonzalez MR, Callaghan PT (2004b) Shear-induced constraint to amphiphile chain dynamics in wormlike micelles (vol 66, pg 132, 2004). Europhys Lett 66:464–464

Hu YT, Lips A (2005) Kinetics and mecahnism of shear banding in an entangled micellar solution. J Rheol 49:1001

Hu YT, Boltenhagen P, Matthys E, Pine DJ (1998a) Shear thickening in low-concentration solutions of wormlike micelles. II Slip, fracture, and stability of the shear–induced phase. J Rheol 42:1209–1226

Hu YT, Boltenhagen P, Pine DJ (1998b) Shear thickening in low-concentration solutions of wormlike micelles. I Direct visualization of transient behavior and phase transitions. J Rheol 42:1185–1208

Hu Y, Wilen L, Philips A, Lips A (2007) Is the constitutive relation for entangled polymers monotonic? J Rheol 51:275

Imaeda T, Furukawa A, Onuki A (2004) Viscoelastic phase separation in shear flow. Phys Rev E 70:051503

Inn YW, Wissbrun KF, Denn MM (2005) Effect of edge fracture on constant torque rheometry of entangled polymer solutions. Macromolecules 38:9385–9388

Johnson M, Segalman D (1977) A model for viscoelastic fluid behavior which allows non-affine deformation. J Non-Newton Fluid Mech 2:255–270

Jou D, Casasvazquez J, Criadosancho M (1995) Thermodynamics of polymer-solutions under flow— phase-separation and polymer degradation. Adv Polym Sci 120:207–266

Kang K, Lettinga MP, Dogic Z, Dhont JKG (2006) Vorticity banding in rodlike virus suspensions. Phys Rev E 74:26307

Keller SL, Boltenhagen P, Pine DJ, Zasadzinski JA (1998) Direct observation of shear-induced structures in wormlike micellar solutions by freeze-fracture electron microscopy. Phys Rev Lett 80:2725–2728

Kishbaugh AJ, McHugh AJ (1993) A rheooptical study of shear-thickening and structure formation in polymer-solutions, 1. Exp Rheol Acta 32:9–24

Kramer L (1981) On the relative stability of states and first-order phase transitions in systems far from equilibrium. Z Phys B 41:357–363

Krug J, Lebowitz JL, Spohn H, Zhang MQ (1986) The fast rate limit of driven diffusive systems. J Stat Phys 44:535–565

Kuzuu N, Doi M (1983) Constitutive equation for nematic liquid crystals under weak velocity gradient derived from a molecular kinetic equation. J Phys Soc Jpn 52:3486–3494

Larson RG (1988) Constitutive equations for polymer melts and solutions. Butterworths, Boston

Larson RG (1992) Instabilities in viscoelastic flows. Rheol Acta 31:213–263

Le TD, Olsson U, Mortensen K, Zipfel J, Richtering W (2001) Nonionic amphiphilic bilayer structures under shear. Langmuir 17:999–1008

Lee JY, Magda J, Hu H, Larson R (2002) Cone angle effects, radial pressure profile, and second normal stress difference for shear-thickening wormlike micelles. J Rheol 46:195

Leon A, Bonn D, Meunier J, Al-Kahwaji A, Greffier O, Kellay H (2000) Coupling between flow and structure for a lamellar surfactant phase. Phys Rev Lett 84:1335–1338

Lerouge S, Argentina M, Decruppe JP (2006) Interface instability in shear-banding flow. Phys Rev Lett 96:088301

Lettinga MP, Dhont JKG (2004) Non-equilibrium phase behaviour of rod-like viruses under shear flow. J Phys Condens Matter 16:S3929–S3939

Likhtman AE, Graham RS (2003) Simple constitutive equation for linear polymer melts derived from molecular theory: Rolie–Poly equation. J Non-Newton Fluid Mech 114:1

Liu AJ, Fredrickson GH (1993) Free energy functionals for semi-flexible polymer solutions and blends. Macromolecules 26:2817

Lopez-Gonzalez MR, Holmes WM, Callaghan PT, Photinos PJ (2004) Shear banding fluctuations and nematic order in wormlike micelles. Phys Rev Lett 93:268302

Lu C-YD, Olmsted PD, Ball RC (2000) The effect of non-local stress on the determination of shear banding flow. Phys Rev Lett 84:642–645

Magda JJ, Lee CS, Muller SJ, Larson RG (1993) Rheology, flow instabilities, and shear-induced diffusion in polystyrene solutions. Macromolecules 26:1696–1706

Malkus DS, Nohel JS, Plohr BJ (1990) Dynamics of shear flow of a non-Newtonian fluid. J Comp Phys 87:464–487

Malkus DS, Nohel JS, Plohr BJ (1991) Analysis of new phenomena in shear flow of non-Newtonian fluids. SIAM J Appl Math 51:899–929

Manneville S, Becu L, Colin A (2004a) High-frequency ultrasonic speckle velocimetry in sheared complex fluids. Eur Phys J Appl Phys 28:361–373

Manneville S, Salmon JB, Colin A (2004b) A spatio-temporal study of rheo-oscillations in a sheared lamellar phase using ultrasound. Eur Phys J E 13:197–212

Manneville S, Colin A, Waton G, Schosseler F (2007) Wall slip, shear banding, and instability in the flow of a triblock copolymer micellar solution. Phys Rev E 75:061502

Marlow SW, Olmsted PD (2002) The effect of shear flow on the helfrich interaction in lyotropic lamellar systems. Eur Phys J E 8:485–497

Marrucci G (1996) Dynamics of entanglements: a nonlinear model consistent with the Cox-Merz rule. J Non-Newton Fluid Mech 62:279–289

Mather PT, Romo-Uribe A, Han CD, Kim SS (1997) Rheo-optical evidence of a flow-induced isotropic-nematic transition in a thermotropic liquid-crystalline polymer. Macromolecules 30:7977–7989

McLeish TCB (1987) Stability of the interface between 2 dynamic phases in capillary-flow of linear polymer melts. J Poly Sci B Poly Phys 25:2253–2264

McLeish T (ed) (1997) In: Proceedings of the NATO advanced study institute on theoretical challenges in the dynamics of complex fluids, Cambridge, UK, vol 339 of E: applied sciences. Kluwer, Dordrecht

McLeish TCB, Ball RC (1986) A molecular approach to the spurt effect in polymer melt flow. J Poly Sci B Poly Phys 24: 1735–1745

Michel E, Appell J, Molino F, Kieffer J, Porte G (2001) Unstable flow and nonmonotonic flow curves of transient networks. J Rheol 45:1465–1477

Milner ST (1993) Dynamical theory of concentration fluctuations in polymer-solutions under shear. Phys Rev E 48: 3674–3691

Milner ST, McLeish TCB, Likhtman AE (2001) Microscopic theory of convective constraint release. J Rheol 45:539–563
Olmsted PD (1999) Two-state phase diagrams for complex fluids in shear flow. Europhys Lett 48:339–345
Olmsted PD, Goldbart PM (1990) Theory of the non-equilibrium phase transition for nematic liquid crystals under shear flow. Phys Rev A41:4578–4581
Olmsted PD, Goldbart PM (1992) Isotropic-nematic transition in shear flow: state selection, coexistence, phase transitions, and critical behavior. Phys Rev A46:4966–4993
Olmsted PD, Lu C-YD (1997) Coexistence and phase separation in sheared complex fluids. Phys Rev E56:55–58
Olmsted PD, Lu C-YD (1999a) Phase separation of rigid rod suspensions in shear flow. Phys Rev E60:4397–4415
Olmsted PD, Lu C-YD (1999b) Phase coexistence of complex fluids in shear flow. Faraday Discuss 112:183–194
Olmsted PD, Radulescu O, Lu C-YD (2000) The Johnson–Segalman model with a diffusion term in cylindrical Couette flow. J Rheol 44:257–275
Panizza P, Colin A, Coulon C, Roux D (1998) A dynamic study of onion phases under shear flow: size changes. Eur Phys J B 4:65–74
Pearson JRA (1994) Flow curves with a maximum. J Rheol 38:309–331
Porte G, Berret JF, Harden JL (1997) Inhomogeneous flows of complex fluids: mechanical instability versus non-equilibrium phase transition. J Phys II 7:459–472 (France)
Pujolle-Robic C, Noirez L (2001) Observation of shear-induced nematic–isotropic transition in side-chain liquid crystal polymers. Nature 409:167–171
Pimenta P, Pashkovski E (2006) Rheology of viscoelastic mixed surfactant solutions: effect of scission on nonlinear flow and rheochaos. Langmuir 22:3980–3987
Radulescu O, Olmsted PD (2000) Matched asymptotic solutions for the steady banded flow of the diffusive Johnson-Segalman model in various geometries. J Non-Newton Fluid Mech 91:141–162
Radulescu O, Olmsted PD, Lu C-YD (1999) Shear-banding in reaction-diffusion models. Rheol Acta 38:606–613
Radulescu O, Olmsted PD, Decruppe JP, Lerouge S, Berret JF, Porte G (2003) Time scales in shear banding of wormlike micelles. Europhys Lett 62:230–236
Raynaud JS, Moucheront P, Baudez JC, Bertrand F, Guilbaud JP, Coussot P (2002) Direct determination by nuclear magnetic resonance of the thixotropic and yielding behavior of suspensions. J Rheol 46:709–732
Rehage H, Hoffmann H (1991) Viscoelastic surfactant solutions—model systems for rheological research. Mol Phys 74:933–973
Rienacker G, Kroger M, Hess S (2002a) Chaotic orientational behavior of a nematic liquid crystal subjected to a steady shear flow. Phys Rev E 66:040702
Rienacker G, Kroger A, Hess S (2002b) Chaotic and regular shear-induced orientational dynamics of nematic liquid crystals. Physica A 315:537–568
Rossi LF, McKinley G, Cook LP (2006) Slippage and migration in Taylor–Couette flow of a model for dilute wormlike micellar solutions. J Non-Newton Fluid Mech 136:79
Roux D, Nallet F, Diat O (1993) Rheology of lyotropic lamellar phases. Europhys Lett 24:53–58
Roux DC, Berret JF, Porte G, Peuvreldisdier E, Lindner P (1995) Shear-induced orientations and textures of nematic wormlike micelles. Macromolecules 28:1681–1687
Salmon JB, Colin A, Roux D (2002) Dynamical behavior of a complex fluid near an out-ofequilibrium transition: approaching simple rheological chaos. Phys Rev E 66: 031505
Salmon JB, Becu L, Manneville S, Colin A (2003a) Towards local rheology of emulsions under Couette flow using dynamic light scattering. Eur Phys J E 10:209–221
Salmon JB, Colin A, Manneville S, Molino F (2003b) Velocity profiles in shear-banding wormlike micelles. Phys Rev Lett 90:228303
Schmitt V, Lequeux F, Pousse A, Roux D (1994) Flow behavior and shear-induced transition near an isotropic-nematic transition in equilibrium polymers. Langmuir 10:955–961
Schmitt V, Marques CM, Lequeux F (1995) Shear-induced phase-separation of complex fluids—the role of flow-concentration coupling. Phys Rev E 52:4009–4015
Schweizer T (2007) Shear banding during nonlinear creep with a solution of monodisperse polystyrene. Rheol Acta 46: 629–637
See H, Doi M, Larson R (1990) The effect of steady flow-fields on the isotropic-nematic phase transition of rigid rod-like polymers. J Chem Phys 92:792–800
Sood AK, Bandyopadhyay R, Basappa G (1999) Linear and nonlinear rheology of wormlike micelles. Pramana J Phys 53:223–235
Spenley NA, Cates ME, McLeish TCB (1993) Nonlinear rheology of wormlike micelles. Phys Rev Lett 71:939–942
Spenley NA, Yuan XF, Cates ME (1996) Nonmonotonic constitutive laws and the formation of shear-banded flows. J Phys II 6:551–571 (France)
Stark E, Lubensky TC (2003) Poisson-bracket approach to the dynamics of nematic liquid crystals. Phys Rev E 67: 61709
Sui C, McKenna GB (2007) Instability of entangled polymers in cone and plate rheometry. Rheol Acta 46:877–888
Tapadia P, Wang SQ (2006) Direct visualization of continuous simple shear in non-Newtonian polymeric fluids. Phys Rev Lett 96:016001
Tapadia P, Ravindranath S, Wang SQ (2006) Banding in entangled polymer fluids under oscillatory shearing. Phys Rev Lett 96:196001
van Egmond JW (1998) Shear-thickening in suspensions, associating polymers, worm-like micelles, and poor polymer solutions. Curr Opin Colloid Interface Sci 3:385–390
Vlassopoulos D, Hatzikiriakos SG (1995) A generalized Giesekus constitutive model with retardation time and its association to the spurt effect. J Non-Newton Fluid Mech 57:119–136
Wang SQ, Drda PA, Inn YW (1996) Exploring molecular origins of sharkskin, partial slip, and slope change in flow curves of linear low density polyethylene. J Rheol 40:875–898
Wang SQ, Ravindranath S, Boukany P, Olechnowicz M, Quirk RP, Halasa A, Mays J (2006) Nonquiescent relaxation in entangled polymer liquids after step shear. Phys Rev Lett 97:187801
Wheeler EK, Fischer P, Fuller GG (1998) Time-periodic flow induced structures and instabilities in a viscoelastic surfactant solution. J Non-Newton Fluid Mech 75:193–208
Wilkins G, Olmsted P (2006) Vorticity banding during the lamellar-to-onion transition in a lyotropic surfactant solution in shear flow. Eur Phys J E 21:133–143
Wilson HJ, Fielding SM (2006) Linear instability of planar shear banded flow of both diffusive and non-diffusive

Johnson-Segalman fluids. J Non-Newton Fluid Mech 138: 181–196

Wunenburger AS, Colin A, Colin T, Roux D (2000) Undulation instability under shear: a model to explain the different orientations of a lamellar phase under shear? Eur Phys J E 2:277–283

Wunenburger AS, Colin A, Leng J, Arneodo A, Roux D (2001) Oscillating viscosity in a lyotropic lamellar phase under shear flow. Phys Rev Lett 86:1374–1377

Yerushalmi J, Katz S, Shinnar R (1970) The stability of steady shear flows of some viscoelastic fluids. Chem Eng Sci 25:1891–1902

Yuan XF (1999) Dynamics of a mechanical interface in shear-banded flow. Europhys Lett 46:542–548

Yuan XF, Jupp L (2002) Interplay of flow-induced phase separations and rheological behavior of complex fluids in shear-banding flow. Europhys Lett 60:691–697

Zilman AG, Granek R (1999) Undulation instability for lamellar phases under shear: a mechanism for onion formation? Eur Phys J B 11:593–608

Zipfel J, Nettesheim F, Lindner P, Le TD, Olsson U, Richtering W (2001) Cylindrical intermediates in a shear-induced lamellar-tovesicle transition. Europhys Lett 53: 335–341